ICIC Express Letters
Volume **17**, Number **7**, July **2023**

ICIC International ©2023 ISSN 1881-803X
pp. **735–740**

GENERATION OF SMOOTH MOIRE-LIKE IMAGES FROM RGB-D IMAGES

Toru Hiraoka

Department of Information Systems
University of Nagasaki
1-1-1, Manabino, Nagayo-chou, Nishisonogi-gun, Nagasaki-ken 851-2195, Japan
hiraoka@sun.ac.jp

Received November 2022; accepted January 2023

Abstract. *A non-photorealistic rendering method has been proposed for automatically generating moire-like images from photographic images using bilateral filter and unsharp mask. In the conventional method, there are areas where it is difficult to generate moire-like patterns, and moire-like patterns may be expressed as angular. Therefore, we apply the extended conventional method to RGB-D images to generate moire-like patterns on the entire image and to express moire-like patterns smoothly. Through experiments using an RGB-D image taken by the authors, the effectiveness of the proposed method was verified. As a result of the experiments, it was found that the proposed method can generate moire-like patterns on the entire image and express it more smoothly than the conventional method.*
Keywords: Non-photorealistic rendering, Moire, Depth, Smooth pattern, Bilateral filter, Unsharp mask

1. **Introduction.** Non-photorealistic rendering (NPR) [1, 2, 3, 4, 5] is a process using computer technology to represent paintings, drawings, cartoons, and items inspired by other sources that do not feature photorealism. Many NPR researches use techniques such as image processing [6, 7] to automatically or semi-automatically generate non-photorealistic images from photographic images, videos, and 3D data. NPR is commonly used on television, movies, websites, and social media.

In this paper, we focus on NPR that automatically generates moire-like images from photographic images [8]. Moire-like images are expressed by superimposing moire-like patterns on photographic images. Iterative processing using bilateral filter [9, 10, 11] and unsharp mask is performed to generate moire-like images. However, the conventional method has problems that there are areas where it is difficult to generate moire-like patterns, and moire-like patterns may be expressed as angular. Therefore, we apply the extended conventional method to RGB-D images to generate moire-like patterns on the entire image and to express moire-like patterns smoothly. A method for generating moire-like images from RGB-D images has also been proposed [12], but the method [12] generates moire-like patterns of a different type of the proposed method and the conventional method [8]. In this paper, moire-like patterns similar to that of the conventional method [8] is generated. To verify the effectiveness of the proposed method, experiments were conducted using RGB-D images taken by the authors.

This paper is organized as follows: the second section describes the proposed method for generating moire-like images from RGB-D images, the third section shows experimental results and reveals the effectiveness of the proposed method, and the conclusion of this paper is given in the fourth section.

DOI: 10.24507/icicel.17.07.735

2. **Proposed Method.** The proposed method is executed in two steps: Step 1 applies bilateral filter embedded the depth, and Step 2 applies unsharp mask using bilateral filter embedded the depth. A flow chart of the proposed method is shown in Figure 1.

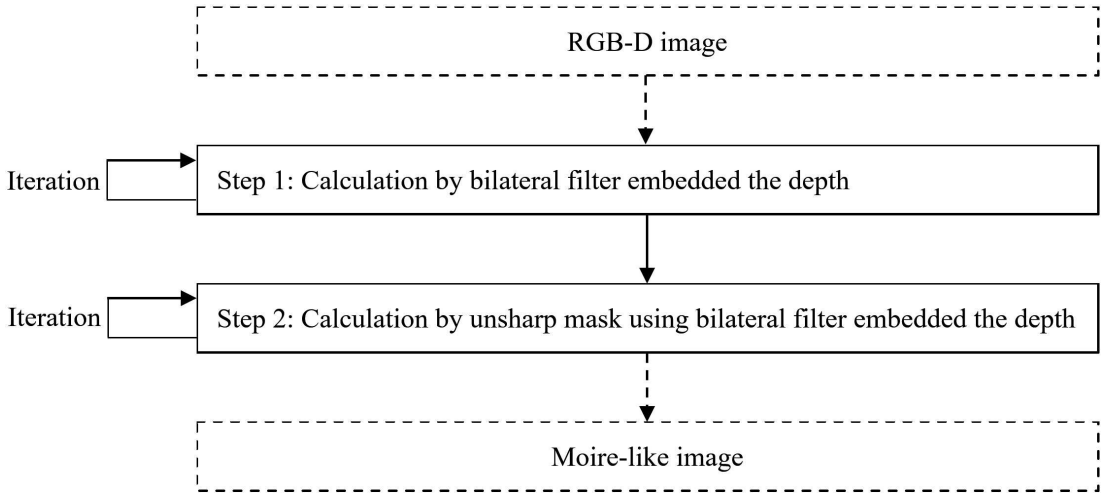

FIGURE 1. Flow chart of the proposed method

Details of the procedure in Figure 1 are explained below.

Step 0: The input pixel values (R, G, B) and the depth for spatial coordinates (i, j) of an RGB-D image are defined as $f_{R,i,j}$, $f_{G,i,j}$, $f_{B,i,j}$, and $f_{D,i,j}$, respectively. The pixel values $f_{R,i,j}$, $f_{G,i,j}$, $f_{B,i,j}$, and $f_{D,i,j}$ have values of U gradations from 0 to $U-1$. The depths $f_{D,i,j}$ are linearly transformed so that the minimum distance becomes 0 and the maximum distance becomes $U-1$.

Step 1: The pixel values and depths of the image at the t-th iteration number are defined as $f^{(t)}_{R,i,j}$, $f^{(t)}_{G,i,j}$, $f^{(t)}_{B,i,j}$, $f^{(t)}_{D,R,i,j}$, $f^{(t)}_{D,G,i,j}$, and $f^{(t)}_{D,B,i,j}$ where $f^{(0)}_{R,i,j} = f_{R,i,j}$, $f^{(0)}_{G,i,j} = f_{G,i,j}$, $f^{(0)}_{B,i,j} = f_{B,i,j}$, $f^{(0)}_{D,R,i,j} = f_{D,i,j}$, $f^{(0)}_{D,G,i,j} = f_{D,i,j}$ and $f^{(0)}_{D,B,i,j} = f_{D,i,j}$. The depths $f^{(t)}_{D,R,i,j}$, $f^{(t)}_{D,G,i,j}$, and $f^{(t)}_{D,B,i,j}$ are the converted values associated with R, G, and B, respectively. The output pixel values $f^{(t)}_{R,i,j}$, $f^{(t)}_{G,i,j}$, $f^{(t)}_{B,i,j}$, $f^{(t)}_{D,R,i,j}$, $f^{(t)}_{D,G,i,j}$, and $f^{(t)}_{D,B,i,j}$ in bilateral filter embedded the depth are calculated by the following equations.

$$f^{(t)}_{R,i,j} = \frac{\sum_{k=i-W}^{i+W}\sum_{l=j-W}^{j+W} e^{-\alpha\left((i-k)^2+(j-l)^2\right)-\beta\max\left(\left(f^{(t-1)}_{R,i,j}-f^{(t-1)}_{R,k,l}\right)^2,\left(f^{(t-1)}_{D,R,i,j}-f^{(t-1)}_{D,R,k,l}\right)^2\right)} f^{(t-1)}_{R,k,l}}{\sum_{k=i-W}^{i+W}\sum_{l=j-W}^{j+W} e^{-\alpha\left((i-k)^2+(j-l)^2\right)-\beta\max\left(\left(f^{(t-1)}_{R,i,j}-f^{(t-1)}_{R,k,l}\right)^2,\left(f^{(t-1)}_{D,R,i,j}-f^{(t-1)}_{D,R,k,l}\right)^2\right)}} \tag{1}$$

$$f^{(t)}_{G,i,j} = \frac{\sum_{k=i-W}^{i+W}\sum_{l=j-W}^{j+W} e^{-\alpha\left((i-k)^2+(j-l)^2\right)-\beta\max\left(\left(f^{(t-1)}_{G,i,j}-f^{(t-1)}_{G,k,l}\right)^2,\left(f^{(t-1)}_{D,G,i,j}-f^{(t-1)}_{D,G,k,l}\right)^2\right)} f^{(t-1)}_{G,k,l}}{\sum_{k=i-W}^{i+W}\sum_{l=j-W}^{j+W} e^{-\alpha\left((i-k)^2+(j-l)^2\right)-\beta\max\left(\left(f^{(t-1)}_{G,i,j}-f^{(t-1)}_{G,k,l}\right)^2,\left(f^{(t-1)}_{D,G,i,j}-f^{(t-1)}_{D,G,k,l}\right)^2\right)}} \tag{2}$$

$$f^{(t)}_{B,i,j} = \frac{\sum_{k=i-W}^{i+W}\sum_{l=j-W}^{j+W} e^{-\alpha\left((i-k)^2+(j-l)^2\right)-\beta\max\left(\left(f^{(t-1)}_{B,i,j}-f^{(t-1)}_{B,k,l}\right)^2,\left(f^{(t-1)}_{D,B,i,j}-f^{(t-1)}_{D,B,k,l}\right)^2\right)} f^{(t-1)}_{B,k,l}}{\sum_{k=i-W}^{i+W}\sum_{l=j-W}^{j+W} e^{-\alpha\left((i-k)^2+(j-l)^2\right)-\beta\max\left(\left(f^{(t-1)}_{B,i,j}-f^{(t-1)}_{B,k,l}\right)^2,\left(f^{(t-1)}_{D,B,i,j}-f^{(t-1)}_{D,B,k,l}\right)^2\right)}} \tag{3}$$

$$f_{D,R,i,j}^{(t)} = \frac{\sum_{k=i-W}^{i+W}\sum_{l=j-W}^{j+W} e^{-\alpha\left((i-k)^2+(j-l)^2\right)-\beta\max\left(\left(f_{R,i,j}^{(t-1)}-f_{R,k,l}^{(t-1)}\right)^2,\left(f_{D,R,i,j}^{(t-1)}-f_{D,R,k,l}^{(t-1)}\right)^2\right)} f_{D,R,k,l}^{(t-1)}}{\sum_{k=i-W}^{i+W}\sum_{l=j-W}^{j+W} e^{-\alpha\left((i-k)^2+(j-l)^2\right)-\beta\max\left(\left(f_{R,i,j}^{(t-1)}-f_{R,k,l}^{(t-1)}\right)^2,\left(f_{D,R,i,j}^{(t-1)}-f_{D,R,k,l}^{(t-1)}\right)^2\right)}} \quad (4)$$

$$f_{D,G,i,j}^{(t)} = \frac{\sum_{k=i-W}^{i+W}\sum_{l=j-W}^{j+W} e^{-\alpha\left((i-k)^2+(j-l)^2\right)-\beta\max\left(\left(f_{G,i,j}^{(t-1)}-f_{G,k,l}^{(t-1)}\right)^2,\left(f_{D,G,i,j}^{(t-1)}-f_{D,G,k,l}^{(t-1)}\right)^2\right)} f_{D,G,k,l}^{(t-1)}}{\sum_{k=i-W}^{i+W}\sum_{l=j-W}^{j+W} e^{-\alpha\left((i-k)^2+(j-l)^2\right)-\beta\max\left(\left(f_{G,i,j}^{(t-1)}-f_{G,k,l}^{(t-1)}\right)^2,\left(f_{D,G,i,j}^{(t-1)}-f_{D,G,k,l}^{(t-1)}\right)^2\right)}} \quad (5)$$

$$f_{D,B,i,j}^{(t)} = \frac{\sum_{k=i-W}^{i+W}\sum_{l=j-W}^{j+W} e^{-\alpha\left((i-k)^2+(j-l)^2\right)-\beta\max\left(\left(f_{B,i,j}^{(t-1)}-f_{B,k,l}^{(t-1)}\right)^2,\left(f_{D,B,i,j}^{(t-1)}-f_{D,B,k,l}^{(t-1)}\right)^2\right)} f_{D,B,k,l}^{(t-1)}}{\sum_{k=i-W}^{i+W}\sum_{l=j-W}^{j+W} e^{-\alpha\left((i-k)^2+(j-l)^2\right)-\beta\max\left(\left(f_{B,i,j}^{(t-1)}-f_{B,k,l}^{(t-1)}\right)^2,\left(f_{D,B,i,j}^{(t-1)}-f_{D,B,k,l}^{(t-1)}\right)^2\right)}} \quad (6)$$

where W is the window size, α and β are positive constants, k and l are the positions in the window, and max() is a function that returns the larger of the two values. The process of Step 1 is repeated T_1 times.

Step 2: The pixel values and depths $f_{R,i,j}^{(T_1)}$, $f_{G,i,j}^{(T_1)}$, $f_{B,i,j}^{(T_1)}$, $f_{D,R,i,j}^{(T_1)}$, $f_{D,G,i,j}^{(T_1)}$, and $f_{D,B,i,j}^{(T_1)}$ are defined as $g_{R,i,j}^{(0)}$, $g_{G,i,j}^{(0)}$, $g_{B,i,j}^{(0)}$, $g_{D,R,i,j}^{(0)}$, $g_{D,G,i,j}^{(0)}$, and $g_{D,B,i,j}^{(0)}$, respectively. The output pixel values $g_{R,i,j}^{(t)}$, $g_{G,i,j}^{(t)}$, $g_{B,i,j}^{(t)}$, $g_{D,R,i,j}^{(t)}$, $g_{D,G,i,j}^{(t)}$, and $g_{D,B,i,j}^{(t)}$ in unsharp mask using bilateral filter embedded the depth are calculated by the following equations.

$$g_{R,i,j}^{(t)} = 2g_{R,i,j}^{(t-1)} - \frac{\sum_{k=i-W}^{i+W}\sum_{l=j-W}^{j+W} e^{-\alpha\left((i-k)^2+(j-l)^2\right)-\beta\max\left(\left(g_{R,i,j}^{(t-1)}-g_{R,k,l}^{(t-1)}\right)^2,\left(g_{D,R,i,j}^{(t-1)}-g_{D,R,k,l}^{(t-1)}\right)^2\right)} g_{R,k,l}^{(t-1)}}{\sum_{k=i-W}^{i+W}\sum_{l=j-W}^{j+W} e^{-\alpha\left((i-k)^2+(j-l)^2\right)-\beta\max\left(\left(g_{R,i,j}^{(t-1)}-g_{R,k,l}^{(t-1)}\right)^2,\left(g_{D,R,i,j}^{(t-1)}-g_{D,R,k,l}^{(t-1)}\right)^2\right)}} \quad (7)$$

$$g_{G,i,j}^{(t)} = 2g_{G,i,j}^{(t-1)} - \frac{\sum_{k=i-W}^{i+W}\sum_{l=j-W}^{j+W} e^{-\alpha\left((i-k)^2+(j-l)^2\right)-\beta\max\left(\left(g_{G,i,j}^{(t-1)}-g_{G,k,l}^{(t-1)}\right)^2,\left(g_{D,G,i,j}^{(t-1)}-g_{D,G,k,l}^{(t-1)}\right)^2\right)} g_{G,k,l}^{(t-1)}}{\sum_{k=i-W}^{i+W}\sum_{l=j-W}^{j+W} e^{-\alpha\left((i-k)^2+(j-l)^2\right)-\beta\max\left(\left(g_{G,i,j}^{(t-1)}-g_{G,k,l}^{(t-1)}\right)^2,\left(g_{D,G,i,j}^{(t-1)}-g_{D,G,k,l}^{(t-1)}\right)^2\right)}} \quad (8)$$

$$g_{B,i,j}^{(t)} = 2g_{B,i,j}^{(t-1)} - \frac{\sum_{k=i-W}^{i+W}\sum_{l=j-W}^{j+W} e^{-\alpha\left((i-k)^2+(j-l)^2\right)-\beta\max\left(\left(g_{B,i,j}^{(t-1)}-g_{B,k,l}^{(t-1)}\right)^2,\left(g_{D,B,i,j}^{(t-1)}-g_{D,B,k,l}^{(t-1)}\right)^2\right)} g_{B,k,l}^{(t-1)}}{\sum_{k=i-W}^{i+W}\sum_{l=j-W}^{j+W} e^{-\alpha\left((i-k)^2+(j-l)^2\right)-\beta\max\left(\left(g_{B,i,j}^{(t-1)}-g_{B,k,l}^{(t-1)}\right)^2,\left(g_{D,B,i,j}^{(t-1)}-g_{D,B,k,l}^{(t-1)}\right)^2\right)}} \quad (9)$$

$$f_{D,R,i,j}^{(t)} = 2g_{D,R,i,j}^{(t-1)} - \frac{\sum_{k=i-W}^{i+W}\sum_{l=j-W}^{j+W} e^{-\alpha\left((i-k)^2+(j-l)^2\right)-\beta\max\left(\left(g_{R,i,j}^{(t-1)}-g_{R,k,l}^{(t-1)}\right)^2,\left(g_{D,R,i,j}^{(t-1)}-g_{D,R,k,l}^{(t-1)}\right)^2\right)} g_{D,R,k,l}^{(t-1)}}{\sum_{k=i-W}^{i+W}\sum_{l=j-W}^{j+W} e^{-\alpha\left((i-k)^2+(j-l)^2\right)-\beta\max\left(\left(g_{R,i,j}^{(t-1)}-g_{R,k,l}^{(t-1)}\right)^2,\left(g_{D,R,i,j}^{(t-1)}-g_{D,R,k,l}^{(t-1)}\right)^2\right)}} \quad (10)$$

$$f_{D,G,i,j}^{(t)} = 2g_{D,G,i,j}^{(t-1)} - \frac{\sum_{k=i-W}^{i+W}\sum_{l=j-W}^{j+W} e^{-\alpha\left((i-k)^2+(j-l)^2\right)-\beta\max\left(\left(g_{G,i,j}^{(t-1)}-g_{G,k,l}^{(t-1)}\right)^2,\left(g_{D,G,i,j}^{(t-1)}-g_{D,G,k,l}^{(t-1)}\right)^2\right)} g_{D,G,k,l}^{(t-1)}}{\sum_{k=i-W}^{i+W}\sum_{l=j-W}^{j+W} e^{-\alpha\left((i-k)^2+(j-l)^2\right)-\beta\max\left(\left(g_{G,i,j}^{(t-1)}-g_{G,k,l}^{(t-1)}\right)^2,\left(g_{D,G,i,j}^{(t-1)}-g_{D,G,k,l}^{(t-1)}\right)^2\right)}} \quad (11)$$

$$f_{D,B,i,j}^{(t)} = 2g_{D,B,i,j}^{(t-1)} - \frac{\sum_{k=i-W}^{i+W}\sum_{l=j-W}^{j+W} e^{-\alpha\left((i-k)^2+(j-l)^2\right)-\beta\max\left(\left(g_{B,i,j}^{(t-1)}-g_{B,k,l}^{(t-1)}\right)^2,\left(g_{D,B,i,j}^{(t-1)}-g_{D,B,k,l}^{(t-1)}\right)^2\right)} g_{D,B,k,l}^{(t-1)}}{\sum_{k=i-W}^{i+W}\sum_{l=j-W}^{j+W} e^{-\alpha\left((i-k)^2+(j-l)^2\right)-\beta\max\left(\left(g_{B,i,j}^{(t-1)}-g_{B,k,l}^{(t-1)}\right)^2,\left(g_{D,B,i,j}^{(t-1)}-g_{D,B,k,l}^{(t-1)}\right)^2\right)}} \quad (12)$$

In case $g^{(t)}_{R,i,j}$, $g^{(t)}_{G,i,j}$, $g^{(t)}_{B,i,j}$, $g^{(t)}_{D,R,i,j}$, $g^{(t)}_{D,G,i,j}$, and $g^{(t)}_{D,B,i,j}$ are less than 0, then $g^{(t)}_{R,i,j}$, $g^{(t)}_{G,i,j}$, $g^{(t)}_{B,i,j}$, $g^{(t)}_{D,R,i,j}$, $g^{(t)}_{D,G,i,j}$, and $g^{(t)}_{D,B,i,j}$ must be set to 0, respectively. In case $g^{(t)}_{R,i,j}$, $g^{(t)}_{G,i,j}$, $g^{(t)}_{B,i,j}$, $g^{(t)}_{D,R,i,j}$, $g^{(t)}_{D,G,i,j}$, and $g^{(t)}_{D,B,i,j}$ are greater than $U-1$, then $g^{(t)}_{R,i,j}$, $g^{(t)}_{G,i,j}$, $g^{(t)}_{B,i,j}$, $g^{(t)}_{D,R,i,j}$, $g^{(t)}_{D,G,i,j}$, and $g^{(t)}_{D,B,i,j}$ must be set to $U-1$, respectively. The process of Step 2 is repeated T_2 times, and an image composed of the pixel values $g^{(T_2)}_{R,i,j}$, $g^{(T_2)}_{G,i,j}$, and $g^{(T_2)}_{B,i,j}$ is the moire-like image of the proposed method.

3. **Experiments.** Experiments were conducted using an RGB-D image which consists of $1280 * 720$ pixels and 256 gradations. A scene of two people in the room was shot using ZED stereo camera. The furthest distance from the camera was 6.289 meters. The RGB-D image is shown in Figure 2. The left and right sides of Figure 2 are the RGB and depth images, respectively. In reference to [8, 12], the values of the parameters T_1, α, β, W, and T_2 used in all experiments were set to 10, 0.01, 0.01, 10, and 20, respectively. The smaller the value of the parameter T_1, the narrower the spacing between moire-like patterns and the finer curve. The smaller the value of the parameter α, the larger the spacing between moire-like patterns. The smaller the value of the parameter β, the less areas where moire-like patterns do not occur and moire-like patterns become clearer. The larger the value of the parameter W, the larger the spacing between moire-like patterns and the more areas where moire-like patterns do not occur. The larger the value of the parameter T_2, the clearer moire-like patterns.

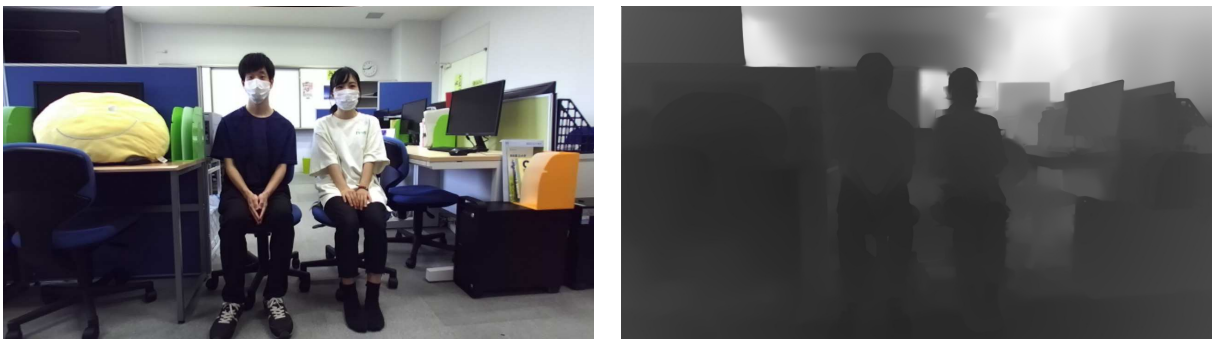

(a) RGB image (b) Depth image

FIGURE 2. RGB-D image

Moire-like images generated by the proposed method and the conventional method [8] were visually evaluated. Moire-like image of the conventional method [8] is shown in Figure 3. The conventional method [8] does not use the depth and uses only RGB values. Looking at Figure 3, it was difficult to generate moire-like patterns in the black areas inside the white ellipses. In addition, moire-like patterns were expressed as angular in the areas inside the white and gray ellipses. Furthermore, the area inside black ellipse is gray except for moire-like patterns.

Moire-like image of the proposed method is shown in Figure 4. Looking at Figure 4, moire-like patterns could be generated even in the black areas that could not be generated by the conventional method. In addition, the moire-like patterns expressed as angular in the conventional method could be expressed more smoothly. Furthermore, the gray area in the conventional method could express in a color closer to that of the original image.

4. **Conclusions.** We proposed an NPR method for automatically generating moire-like images from RGB-D images. The proposed method is characterized by being able to generate moire-like patterns on the entire image and to express moire-like patterns smoothly. Through experiments using an RGB-D image taken by the authors, the appearance of

FIGURE 3. Moire-like image of the conventional method

FIGURE 4. Moire-like image of the proposed method

moire-like images generated by the conventional and proposed methods was evaluated visually. As a result of the experiments, it was found that the proposed method can generate moire-like patterns on the entire image and express it more smoothly than the conventional method.

The future task is to apply the proposed method to more RGB-D images, although this paper applied the proposed method to one type of RGB-D image.

Acknowledgment. This work was supported by JSPS KAKENHI Grant Number JP19K 12664.

REFERENCES

[1] J. Lansdown and S. Schofield, Expressive rendering: A review of nonphotorealistic techniques, *IEEE Computer Graphics and Applications*, vol.15, no.3, pp.29-37, 1995.

[2] D. Martin, G. Arroyo, A. Rodriguez and T. Isenberg, A survey of digital stippling, *Computers & Graphics*, vol.67, pp.24-44, 2017.

[3] I. Ilinkin, Designing a course on non-photorealistic rendering, *Eurographics*, pp.9-16, 2020.

[4] P. L. Rosin, Y. K. Lai, D. Mould, R. Yi, I. Berger, L. Doyle, S. Lee, C. Li, Y. J. Liu, A. Semmo, A. Shamir, M. Son and H. Winnemoller, NPRportrait 1.0: A three-level benchmark for non-photorealistic rendering of portraits, *Computational Visual Media*, vol.8, no.3, pp.445-465, 2022.
[5] B. Li, Z. Luo and B. Mao, Non-photorealistic visualization of 3D city models using visual variables in virtual reality environments, *Procedia Computer Science*, vol.214, pp.1516-1521, 2022.
[6] J. Chen, J. Tang, F. Zhang, H. Ni and Y. Tang, A novel digital color image encryption algorithm based on a new 4-D hyper-chaotic system and an improved S-box, *International Journal of Innovative Computing, Information and Control*, vol.18, no.1, pp.73-92, 2022.
[7] Y. Zhao and Q. Huang, Image enhancement of robot welding seam based on wavelet transform and contrast guidance, *International Journal of Innovative Computing, Information and Control*, vol.18, no.1, pp.149-159, 2022.
[8] T. Hiraoka and K. Urahama, Generation of moire-picture-like color images by bilateral filter, *IEICE Transactions on Information and Systems*, vol.E96-D, no.8, pp.1862-1866, 2013.
[9] C. Tomasi and R. Manduchi, Bilateral filtering for gray and color images, *Proc. of ICCV*, pp.839-846, 1998.
[10] S. Paris, P. Kornprobst, J. Tumblin and F. Durand, Bilateral filtering: Theory and applications, *Foundations and Trends in Computer Graphics and Vision*, vol.4, no.1, pp.1-73, 2008.
[11] S. W. Cheng, Y. T. Lin and Y. T. Peng, A fast two-stage bilateral filter using constant time $O(1)$ histogram generation, *Sensors*, vol.22, no.3, pp.1-11, DOI: 10.3390/s22030926, 2022.
[12] R. Takaki and T. Hiraoka, Generation of moire-like images from RGB-D images, *ICIC Express Letters*, vol.15, no.1, pp.37-42, 2021.